ACS APPLIED BIO MATERIALS

Subscriber access provided by DCU Library

Article

Microcavity Supported Lipid Membranes: Versatile Platforms for Building Asymmetric lipid bilayers and for Protein Recognition

Guilherme Batista Berselli, Nirod Kumar Sarangi,
Sivaramakrishnan Ramadurai, Paul V. Murphy, and Tia E. Keyes

ACS Appl. Bio Mater., **Just Accepted Manuscript** • DOI: 10.1021/acsabm.9b00378 • Publication Date (Web): 27 Jun 2019

Downloaded from http://pubs.acs.org on July 3, 2019

Just Accepted

“Just Accepted” manuscripts have been peer-reviewed and accepted for publication. They are posted online prior to technical editing, formatting for publication and author proofing. The American Chemical Society provides “Just Accepted” as a service to the research community to expedite the dissemination of scientific material as soon as possible after acceptance. “Just Accepted” manuscripts appear in full in PDF format accompanied by an HTML abstract. “Just Accepted” manuscripts have been fully peer reviewed, but should not be considered the official version of record. They are citable by the Digital Object Identifier (DOI®). “Just Accepted” is an optional service offered to authors. Therefore, the “Just Accepted” Web site may not include all articles that will be published in the journal. After a manuscript is technically edited and formatted, it will be removed from the “Just Accepted” Web site and published as an ASAP article. Note that technical editing may introduce minor changes to the manuscript text and/or graphics which could affect content, and all legal disclaimers and ethical guidelines that apply to the journal pertain. ACS cannot be held responsible for errors or consequences arising from the use of information contained in these “Just Accepted” manuscripts.

is published by the American Chemical Society. 1155 Sixteenth Street N.W.,
Washington, DC 20036

Published by American Chemical Society. Copyright © American Chemical Society.
However, no copyright claim is made to original U.S. Government works, or works
produced by employees of any Commonwealth realm Crown government in the course
of their duties.

Microcavity Supported Lipid Membranes: Versatile Platforms for Building Asymmetric lipid bilayers and for Protein Recognition

Guilherme B. Berselli,[1] *Nirod Kumar Sarangi*[1]*, Sivaramakrishnan Ramadurai*[1]*, Paul V. Murphy,*[2] *Tia E. Keyes*[1]**

[1]School of Chemical Sciences and National Biophotonics and Imaging Platform, Dublin City University, Dublin 9, Ireland.

[2]School of Chemistry NUI Galway University Road, Galway Ireland.

*E-mail: tia.keyes@dcu.ie

ABSTRACT. Microcavity supported lipid bilayers (MSLB) are contact-free membranes suspended across aqueous-filled pores that maintain the lipid bilayer in a highly fluidic state and free from frictional interactions with substrate. Such platforms offer the prospect of liposome-like fluidity with the compositional versatility and addressability of supported lipid bilayers and thus offer significant opportunity for modelling membrane asymmetry, protein-membrane interactions and aggregation at the membrane interface. Herein, we evaluate their performance by studying the effect of transmembrane lipid asymmetry on lipid diffusivity, membrane viscosity and cholera toxin- ganglioside recognition across six symmetric and asymmetric membranes including binary compositions containing both fluid and gel phase, and ternary phase separated membrane compositions. Fluorescence lifetime correlation spectroscopy (FLCS) was used to determine the lateral mobility of lipid and protein, and electrochemical impedance spectroscopy (EIS) enabled detection of protein-membrane assembly over the nanomolar range. Transmembrane leaflet asymmetry was observed to have profound impact on membrane electrochemical resistance where the resistance of a ternary symmetric phase separated bilayer was found to be at least 2.6 times higher than the asymmetric bilayer with analogous composition at the distal leaflet but where the lower leaflet comprised only 1,2-dioleoyl-*sn*-glycero-3-phosphocholine (DOPC). Similarly, the diffusion coefficient for MSLBs was observed to be 2.5 fold faster for asymmetric MSLBs where the lower leaflet is DOPC alone. Our results demonstrate that interplay of lipid packing across both membrane leaflets and concentration of GM1 both affect the extent of cholera toxin aggregation and consequent diffusion of the cholera-GM1 aggregates. Given that true biomembranes are both fluidic and asymmetric, MSLBs offer the opportunity for building greater biomimicry into biophysical models and the approach described demonstrates the value of MSLBs in studying aggregation and membrane associated multivalent interactions prevalent in many carbohydrates mediated processes.

keywords: microcavity supported lipid bilayer, protein-glycolipid interaction, microcavity array, membrane asymmetry, cholera toxin, GM1, electrochemical impedance spectroscopy, fluorescence lifetime correlation spectroscopy

INTRODUCTION

Artificial lipid membranes are indispensable tools for evaluating biophysical processes, such as membrane permeation, protein recognition and aggregation, under conditions of controlled lipid composition.[1] They can provide a means to disentangle insights into unit membrane processes from the confounding complexity of the cell.[2] A good artificial model will have controllable lipid composition, good stability and critically, will maintain high membrane lateral fluidity.[3–5] Also, ideally, in the interests of biomimicry, the membrane should be asymmetric. The plasma membrane is naturally asymmetric, the lipid composition of the mammalian membrane for instance, contains predominantly phosphatidylcholine (PC) and other choline derivatives, glycolipids and sphingomyelin (SM) at the exterior leaflet, whereas the cytoplasmic leaflet contains phosphoethanolamine (PE), negatively charged lipids such as phosphatidylserine (PS) and other amino lipids. Cholesterol is contained within and is mobile across both leaflets.

The asymmetry is thought to lead to significant differences in phase behavior and diffusivity of each leaflet of the plasma membrane. In particularly the predominance of SM at the outer leaflet leads to the coexistence of liquid ordered (L_o) and liquid disordered (L_d) and gel phases, whereas model distal leaflets have shown no evidence of such domain formation. Thus it is likely that there is a significant disparity in the fluidity of each of the plasma membrane leaflets. Furthermore, transmembrane lipid asymmetry and inter-leaflet coupling have been reported to play a crucial role in plasma membrane function and organization, where evidence suggests that inter-leaflet coupling and domain registration lead each leaflet to be profoundly influenced by the composition of its neighbour.[6,7] This effect has been predicted widely in computational simulations, but experimental investigations into the influence of asymmetry/symmetry of lipid membranes on lipid-leaflet coupling and mobility are relatively uncommon.[8–10] Presumably, because of challenges in building model systems at which asymmetry and lateral fluidity can be simultaneously accomplished.[8,11,12]

Liposomes and supported lipid bilayers (SLBs) are some of the most widely applied artificial cell membrane models. However, they respectively preclude reliable attainment of controlled asymmetric composition and optimal fluidity.[6,13] In the latter case, asymmetric supported lipid bilayers (aSLBs) are readily accessible using controlled lipid deposition techniques to assemble, independently, two lipid monolayers[9] or by lipid translocation using chemical or mechanical lipid redistribution after vesicle fusion to a planar substrate.[10,14,15] However, frictional interactions between the lower (proximal) leaflet and the substrate hinder lateral diffusion in these and related tethered or polymer cushioned bilayers. Therefore, lipid and reconstituted protein mobility in asymmetric cell membrane models have not been widely explored using such models.

An alternative approach to emerge in recent years is porous-supported membrane structures where the lipid membrane is supported in part over air or fluid.[16–19] In the former case, stable bilayers typically require nano-pore dimensions but where aqueous filled supports are used, the bilayer can be suspended over pores of multiple microns. Recently, we demonstrated that lipid bilayers supported above aqueous filled micron-sized spherical pore arrays in gold and in poly(dimethylsiloxane) (PDMS) are stable and produce highly fluidic bilayers simulating the behavior of liposome. The micron dimensioned pores are attractive as they are amenable to microscopy, enabling single pores to be individually interrogated. Across arrays, this can lead to robust statistical reliability of results. When prepared in gold, the arrays can work as an electrode permitting electrochemical interrogation of membrane behavior.[20] Such stable microarray supported bilayers hold great potential as analytical devices for protein binding and detection.[21]

Cholera Toxin recognizes, specifically, the monosialosyl ganglioside GM1 at the plasma membrane of the gut epithelia through its subunit b (CTb). This membrane localized recognition is the first step in a process that permits the toxin to gain access to the endoplasmic reticulum. CTb-GM1 association is a multivalent process that has been studied at a variety of membrane models and has been applied to evaluate new lipid-protein platform models for protein detection.[21–24] In complex and phase separated lipid compositions and at the cell membrane, a number of studies have demonstrated that CTb associates at the L_o phase, and that CTb stabilizes raft domains via a lipid-crosslinking.[25,26] However, to date, the impact, of lipid membrane asymmetry on CTb-GM1 association has not been considered in detail, although in true biological membranes, as described, the bilayers are highly asymmetric.

Using MSLBs, herein, we examine the impact of lipid composition and asymmetry on cholera toxin-GM1 recognition and aggregation using fluorescence lifetime correlation spectroscopy

(FLCS) and electrochemical impedance spectroscopy (EIS). A simple and versatile method was utilized to build transversally asymmetric lipid bilayer using a hybrid Langmuir Blodgett-vesicle fusion (LB-VF) lipid assembly.[18,20] Using FLCS, we first examined the lateral diffusion of labeled lipid marker within different asymmetric and symmetric lipid systems and then we addressed the impact of lipid bilayer asymmetric compositions on CTb-glycosphingolipid(GSL) binding and mobility. The relatively high fluidity of the asymmetric bilayer compositions enabled us to study diffusion of cholera toxin aggregates at phase separated bilayers rendered impossible at symmetric compositions due to slow diffusion/photobleaching of the labels. The observations reflect the influence of complex lipid composition on the lateral aggregation of CTb at GM1 containing bilayers. EIS succinctly corroborate the CTb detection to the GM1 containing membrane, implying transmembrane asymmetry and lipid composition support such interaction and binding. Overall, our results demonstrate the utility of microfluidic cavity array supported bilayers as a versatile platform for the assembly and study of asymmetric lipid compositions and for evaluation of biologically important multivalent binding systems and protein aggregation at ligand containing membranes.

EXPERIMENTAL SECTION

Materials

1,2-dioleoyl-*sn*-glycero-3-phosphocholine (DOPC), porcine brain N-(octadecanoyl)-sphing-4-enine-1-phosphocholine (SM), cholesterol and ganglioside GM1 were purchased with maximum degree of purity (> 99%) from Avanti Polar Lipids (Alabama, USA) and used without further purification. 1,2-dioleoyl-*sn*-glycero-3-phosphoethanolamine labeled Atto655 (DOPE-A655) was purchase from ATTO-TEC GmbH (Siegen, Germany). Conjugated B subunit cholera toxin labeled Alexa 555 (CTb-A555) was purchased from Invitrogen (Thermo Fisher). Free unlabeled B subunit cholera toxin (CTb) and phosphate buffer saline (PBS) tablets were purchased from Sigma-Aldrich (Wicklow, Ireland). Aqueous solutions were prepared using Milli-Q water (Millipore Corp., Bedford, USA). Polydimethylsiloxane silicon elastomer (PDMS) was purchased from Dow Corning GmbH (Wiesbaden, Germany) and mixed following supplier instructions. Silicon wafers coated with a 100 nm layer of gold on a 50 Å layer of titanium were obtained from AMS Biotechnology Inc. The monodisperse polystyrene latex sphere with a diameter of 1 μm was obtained from Bangs Laboratories Inc. The commercial cyanide free gold plating solution (TG-25 RTU) was obtained from Technic Inc. All other HPLC grade reagents were obtained from Sigma-Aldrich and used as obtained.

Gold and PDMS microcavity array preparation

The lipid bilayers were suspended across buffer-filled PDMS or gold microcavity arrays prepared according to protocols previously described by our group.[18] Briefly, for FCS, the microcavity array was prepared by drop casting 50 μL of ethanol containing 0.1% of 4.61 μm polystyrene spheres (Bangs Laboratories) onto a 1 cm x 1 cm hand cleaved mica sheet. After ethanol evaporation, PDMS was poured onto the PS spheres array and cured at 90 °C for 1h. The microcavities array is then formed after removing the inserted PS spheres by sonicating the PDMS substrate in tetrahydrofuran (THF) for 15 min. The substrates were then left to dry overnight. Prior to lipid bilayer formation, the substrates were plasma cleaned using oxygen plasma for 5 min and microcavities were buffer filled before to lipid monolayer deposition by sonicating PDMS substrate in PBS buffer (pH 7.4) for 1h. As previously reported, this step is important to increase the hydrophilicity of the substrate.[18]

For electrochemical studies, lipid bilayers were suspended across gold microcavity arrays prepared by microsphere lithography and selectively modified with a self-assembled monolayer (SAM) of 1 mM 6-Mercapto-1-hexanol (MH) as described previously.[20,27] The detailed description for the preparation of microcavity array and MSLBs are presented in the supplementary information (Figs. S1 and S2).

Preparation of Large Unilamellar Vesicles (LUVs)

In this work, liposome fusion was used to form the distal lipid leaflet on MSLB's. To prepare the liposomes, stock solutions of all vesicle components such as DOPC, brain sphingomyelin (SM) and cholesterol (Chol) 50 mg/ml each, and GM1 (1 mg/ml) were prepared in chloroform and stored in sealed glass vials at -20°C. For fluorescence studies, unlabeled lipids and fluorescently labeled phospholipid DOPE-A655 were mixed in a ratio of 50000:1 mol/mol. For electrochemical measurements, as EIS is label-free, the probe was not included during the preparation of MSLBs. Aliquots of the appropriate amounts of the stock solutions were mixed in clean amber glass vials and the chloroform was removed under a gentle stream of nitrogen to form a thin layer lipid coating on glass vials. To ensure complete removal of residual chloroform, the lipids thin films were placed under vacuum for at least 3 h and then the lipids were rehydrated in 1 ml of PBS buffer and vortexed vigorously for 60 s. A mini-extruder (Avanti Polar Lipids) was used to extrude the multilamellar vesicles suspension through a polycarbonate membrane (0.1 μm pore size). The resulting large unilamellar vesicles (LUV) (approximately 100 nm diameter) solution was diluted to 0.25 mg/ml. Liposomes composed of SM were extruded at 45°C, above the SM transition temperature, to guarantee that vesicles are in the fluidic state.

Microcavity Supported Lipid Bilayers (MSLB) preparation

To assemble suspended asymmetric/symmetric lipid bilayer membranes across pre-buffer filled microcavity arrays of both PDMS and gold substrates, a hybrid two-step method, Langmuir-Blodgett lipid transfer followed by vesicle fusion (LB-VF) method was employed.[18] Briefly, a spanned lipid monolayer is first deposited onto the microcavity substrate by LB transfer (LB trough; KSV Nima Model 102M) with Milli-Q water as the subphase. Lipid solution (50 μL, 1 mg/ml in chloroform) was added dropwise gently over 2-3 min on the subphase of LB trough and allowed solvent to evaporate for 15 min. Prior to the preparation of proximal leaflet monolayer using LB method, multiple compression-expansion cycles were followed before the collapse surface pressure and subsequently the monolayers were transferred at a highly condensed surface pressure of 32 mNm^{-1} by the vertical withdrawal of submerged substrate at a speed of 15 mm/min to get an adequate transfer ratio (TR) of 1 (Fig. S3). To form supported lipid bilayer, the monolayer-coated gold substrate was dipped in LUV solution for 30 min for fusion and then washed with PBS buffer and stored in PBS until further use. Prior to liposome fusion on to the monolayer coated PDMS thin chamber, the substrate was sealed to cover glass with rapid adhesive glue (Araldite). The microfluidic device was formed after insertion of two silicon tubes to the sealed chamber containing the microcavity array by punching two holes through the PDMS into cavity chamber (see SI, Fig. S4). To remove residual/unreacted liposomes, the microfluidic device was purged with 1 ml of PBS buffer (pH 7.4). Care was taken to ensure that at no stage during the preparation or measurements the bilayer was exposed to air. In this work, the proximal leaflet refers to the LB deposited lipid leaflet next to the substrate and the distal leaflet is the outer lipid layer facing toward the bulk solution.

Electrochemical impedance spectroscopy (EIS)

Electrochemical impedance measurements were performed on a CHI 760B bipotentiostat (CH Instruments Inc., Austin, TX) in a three-electrode cell consisting of a Ag/AgCl (1 M KCl) reference electrode, platinum coiled wire as a counter electrode and the gold substrate with microcavity array served as the working electrode. Impedance measurements were performed in the presence of 1 mM $K_3[Fe(CN)_6]$/ $K_4[Fe(CN)_6]$ (1:1 mol/mol) mixture, used as a redox probe dissolved in PBS buffer containing additional 0.1 M KCl as supporting electrolyte. The EIS were recorded in the frequency region of 10^4 and 0.01 Hz with a bias potential of 0.26 V vs Ag/AgCl. The impedance spectra were fit to an equivalent circuit as previously described.[20] In the circuit, R_S is the solution resistance, R_M and CPE_M represents the resistance and constant phase element of the membrane and R_C and CPE_C represents the cavity resistance and constant phase element of the gold substrate. The constant phase elements (CPE) were used in the equivalent circuit to provide to account for the heterogeneity of the SLBs in microcavity array. The impedance of the CPE can be calculated using Eq. (1);

$$Z_{CPE} = \frac{1}{Q(j\omega)^{\beta}} \tag{1}$$

where Q and the exponent β represent respectively the CPE and an empirical constant related to the frequency dispersion.

Fluorescence Lifetime Correlation Spectroscopy (FLCS)

Single point FLCS was used to assess both the lipid membrane fluidity and change in response to CTb binding to GM1. FLCS measurements were performed on a MicroTime 200 lifetime (PicoQuant GmbH, Berlin, Germany) using a water immersion objective (NA 1.2 UPlanSApo 60 x 1.2 CC1.48, Olympus). The detection unit comprises of two single photon avalanche diode (SPAD) from PicoQuant. Labeled lipid membrane marker DOPE-A655 was excited with 640 nm LDH-P-C-640B (PicoQuant) and CTb-A555 was excited with 532 nm PicoTA laser from Toptica (PicoQuant). To exclude scattered or reflected laser light, emitted fluorescence was collected through a HG670lp AHF/Chroma or HQ550lp AHF/Chroma band pass filter for 640 or 532 nm laser respectively. A 50 μm pinhole was used to eliminate photons from outside the confocal volume. Before FCLS measurement, backscattered images of the substrate were taken using an OD3 density filter to ensure optimal positioning of the focus to the centre of the microcavity. Then, the bilayer position was determined by z-scanning until the point of maximal fluorescence intensity of DOPE-A655 was found. At this point, the fluctuating fluorescence intensity of labeled lipid marker or CTb-A555 were measured for 30 to 60 seconds per cavity, and replicate data from 20 to 30 cavities were measured per sample. To assess simultaneously the diffusion time (ms) and the fluorescence lifetime (ns) the emitted photons were analyzed by a time-correlated single photon counting system (TCSPC) (PicoHarp 300 from Picoquant).[28] The fluorescence fluctuations obtained are then correlated with a normalized autocorrelation function (Equation 2):

$$G(\tau) = \frac{\langle \delta F(t).\delta F(t+\tau) \rangle}{\langle F(t) \rangle^2} \qquad (2)$$

The auto-correlation curves obtained from the fluorescence fluctuations were fitted to a 2-D model (Equation 3) using the software SymphoTime (SPT64) version 2.2 (PicoQuant).

$$G(\tau) = \frac{1}{N(1-T)}\left[1 - T + Te^{\left(-\frac{\tau}{\tau_T}\right)}\right]\left[1 + \left(\frac{\tau}{\tau_D}\right)^{\alpha}\right]^{-1} \qquad (3)$$

Some autocorrelation data fit best to a 2D diffusion model for two diffusing moieties where a a second component was included in to equation 3, to give equation 4.

$$G(\tau) = \frac{1}{N(1-T)}\left[1 - T + Te^{\left(-\frac{\tau}{\tau_T}\right)}\right]\left[1 + \left(\frac{\tau}{\tau_{D1}}\right)^{\alpha 1}\right]^{-1}\left[1 + \left(\frac{\tau}{\tau_{D2}}\right)^{\alpha 2}\right]^{-1} \qquad (4)$$

Here, ρ represents the amplitude at G(τ) and is defined as the inverse of number of molecules (1/N), T corresponds to the fraction of molecules at triplet “dark” state, τ_{trip} is the triple state time and α is the anomalous parameter; τ_D is the diffusion time of the molecules and τ_T is the decay time for the triplet state. The diffusion coefficient is related to the correlation time τ_D by the relation $D = \omega^2/4\tau_D$, where ω is the $1/e^2$ radius of the confocal volume i.e. the waist of the exciting laser beam. ω was measured for each excitation using a reference solution of free dye for which the diffusion coefficient is known. The ω was determined by calibration using reference dyes; Atto 655 (Atto TEC, GmbH) for 640nm laser and Rhodamine 6G for 532 nm laser at 20°C in water. Detailed description of the experimental set up can be found in Figure S4.

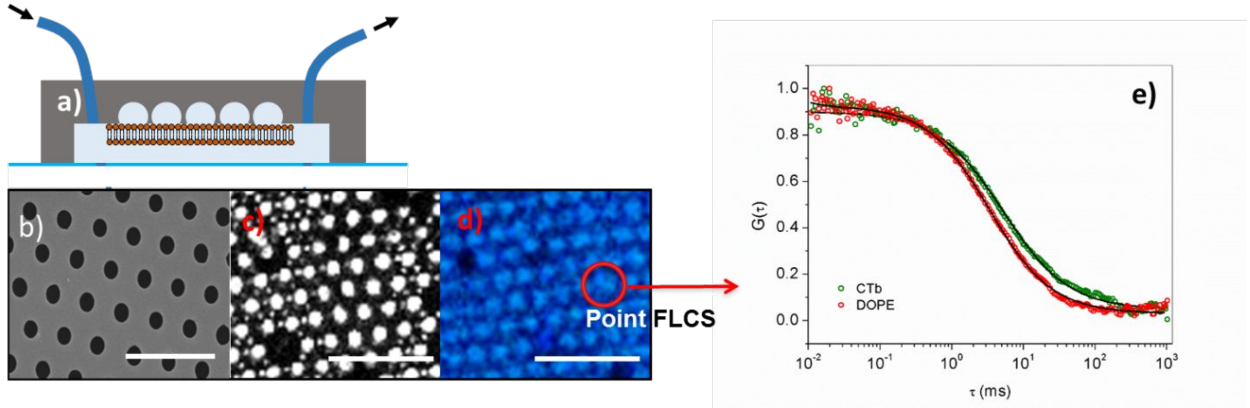

Figure 1. a) Schematic of the microfluidic platform made of PDMS. b) SEM image of cured PDMS microcavity array before buffer spanning a lipid bilayer made by pouring the polymer to 4.6 μm diameter polystyrene spheres before assembling the microfluidic device. c) reflectance image obtained using a OD3 density filter after lipid bilayer deposition. d) Fluorescence lifetime image of labeled DOPE-A655 of an asymmetric DOPC (proximal leaflet) // DOPC/GM1 (1 mol%) (distal leaflet) lipid bilayer. The scale bar is 10μm. e) Typical FLCS autocorrelation data of labeled DOPE (red) and CTb (green) over a microcavity. Solid lines represent the 2D fitting to equation (3).

Due to the suspended character of planar MSLBs, where both leaflets are in contact with bulk aqueous phase, we can assume the Saffman-Delbrück model (Equation 5) applies and use it to estimate the membrane viscosity from lateral diffusion values obtained for labeled DOPE-A655:

$$D = \frac{KT}{4\pi\mu h}\left(\ln\left(\frac{\mu h}{\mu' r}\right) - \gamma\right) \tag{5}$$

Where D is the lateral diffusion obtained from FLCS, K is Boltzmann constant, T is the absolute temperature, r is the radius of the cylindrical membrane inclusion, h is the membrane thickness, γ is Euler-Mascheroni constant (approx. 0.577), μ and μ' are the membrane viscosity and the bulk solution viscosity, respectively. The parameters used to estimate the membrane μ were: radius of the inclusion r = 0.1 nm, membrane height h = 3.8 nm and the viscosity of the surrounding media μ' = 0.001 Pa.s.

RESULTS AND DISCUSSION

Preparation of transversally asymmetric microcavity supported lipid bilayers

The eukaryotic cell membrane has a transversally asymmetric lipid distribution and this characteristic has important biophysical consequences in natural systems.[5] A key advantage of the microcavity supported lipid membrane is that it is readily amenable to the preparation of asymmetric lipid bilayer compositions in a manner similar to supported lipid membranes but with the key difference that the MSLBs retains the fluidity of a liposome membrane. To investigate the influence of transmembrane asymmetry on lipid diffusivity, the MSLBs were prepared using a hybrid LB-VF method, so that the proximal leaflet (array substrate side) comprised of DOPC while the distal leaflet comprised of either DOPC, DOPC:SM (1:1) or DOPC:SM:Chol (2:2:1). Note that 1% (mol:mol) GM1 was added in each case only to the distal leaflet as a receptor to CTb. The labeled lipid DOPE-A655 used as a fluorescent marker at 0.01 mol% was inserted only into the distal leaflet. A schematic representation of the MSLB's on buffer filled microcavities and the microcavity array are shown in Figure 1a and b, respectively.

As the asymmetric lipid bilayers are in a non-equilibrium state, and it is expected, that composition will gradually equilibrate. In cholesterol-containing asymmetric compositions, cholesterol can flip-flop to the proximal leaflet rapidly.[29] However, numerousstudies at SLBs indicate that lipid asymmetry is maintained for many hours.[9,10,30] To confirm that asymmetry was maintained during our experimental windows we evaluated the diffusion coefficient of the outer leaflet over 5 hours following assembly and found that negligible change had occurred (Fig. S4 (iv and v), supplemental materials). Because of the large difference between diffusivity of the DOPC and mixed composition monolayers if significant mixing/flip-flop were occurring over this time-scale we would expect to see significant modification to the diffusion coefficient or biphasic behavior if the probe were flip-flopping. To mitigate against any loss of asymmetry, measurements were completed in the present studies immediately following bilayer preparation and were completed within 3 to 4 hours.

Confocal imaging of DOPE-A655 labeled MSLB's confirm continuous lipid bilayer spanning the PDMS microcavities are formed for all lipid compositions (Figure 1c and 1d). Occasionally unfilled cavities occur but these are easily distinguished as "dark spots" caused by the absence of lipid membrane at pores that have failed to fill with water and where consequently, bilayers tend to be unstable at the air interface across such large pores. Without the lipid marker DOPE-A655 present in the bilayers, no background fluorescence was observed from the PDMS platform or bilayers (see SI). To avoid contributions from diffusion of lipid bilayer over the flat regions of array, all measurements are performed at a buffer encapsulated cavity by focusing first with the reflectance image on a single aqueous filled pore before Z-scanning to focus on the bilayer and acquiring the FLCS autocorrelation function (ACF). Representative FLCS data from a cavity spanned DOPC membrane labeled with DOPE-A655 is shown in Figure 1e (open red symbol). The lateral diffusion is calculated after fitting the obtained ACF with equation 3 (solid line, Figure 1e).

Transmembrane lipid symmetry affects the lipid membrane fluidity and viscosity

The diffusivity of DOPE-A655 at MSLBs with different asymmetric and symmetric MSLBs were extracted (Table 1) and plotted against lipid composition (Figure 2). A set of DOPE-A655 ACFs obtained above asymmetric and symmetric lipid bilayers spanned above microcavities is displayed in Figure S4vi. The lateral diffusion coefficient obtained for a DOPC lipid bilayer was approximately 10 $\mu m^2 s^{-1}$, which is consistent with previously reported values for DOPC MSLBs as well as for reported free-standing DOPC bilayers.[18,31]

As expected, the composition of the bilayer, has a profound effect on diffusivity. For instance, upon addition of SM to the distal leaflet of the MSLBs so that it comprises 1:1 mol/mol DOPC/SM, where the proximal leaflet is DOPC alone, DOPE-A655 lateral diffusion in the distal leaflet reduces to 5.37 ± 0.75 $\mu m^2 s^{-1}$. The reduced fluidity of the bilayer is attributed to the presence of enriched SM gel-phases that increase the distal layer viscosity. Indeed, reports of diffusion of analogous compositions in symmetric silicate-supported SLBs show that diffusion is suppressed.[32] The inclusion of cholesterol (Chol) in the asymmetric MSLBs so that the distal leaflet comprises DOPC/SM/Chol (2:2:1) increases DOPE-A655 diffusion to 8.66 ± 2.53 $\mu m^2 s^{-1}$ as compared to the diffusivity values of DOPC/SM(1:1) asymmetric bilayer. This is consistent with numerous previous reports[33], including that of Yokota and Ogino who demonstrated that introduction of Chol into DOPC/SM (1:1) transitions the membrane from co-existing gel and fluid phases in SLBs to mixed phases of liquid disordered (L_d) domains rich in DOPC and micron-sized liquid ordered (L_o) domains rich in SM and cholesterol.[32] The formation of L_o domains are thought to be promoted by hydrogen bonding interactions between SM tails and cholesterol[34–36] and the increase in fluidity reported is attributed to the preferential partitioning of labeled DOPE to L_d phase.[34]

Table 1. Diffusion coefficient of labeled DOPE at the distal layer of MSLBs and calculated membrane viscosity for different lipid compositions using Saffman-Delbrück model. The viscosity values obtained from DOPE diffusion lie within ranges previously reported for lipid bilayers at 20±0.5 °C.

lipid composition	DOPE diffusion ($\mu m^2 s^{-1}$)	calculated μ (Pa.s)
Sym DOPC + GM1 (1 mol%)	10.0 ± 0.84	0.05 ± 0.006

Asym DOPC/SM/Chol (2:2:1) + GM1 (1 mol%)	8.66 ± 2.53	0.06 ± 0.01
Asym DOPC/SM (1:1) + GM1 (1 mol%)	5.37 ± 0.75	0.10 ± 0.005
Sym DOPC/SM/Chol (2:2:1) + GM1 (1 mol%)	3.34 ± 0.67	0.15 ± 0.003
Sym DOPC/SM (1:1) + GM1 (1 mol%)	1.52 ± 0.69	0.40 ± 0.003

To compare the fluidity of asymmetric and symmetric bilayers, we prepared symmetric MSLBs using the LB-VF method; where both LB and LUVs had the same composition, but GM1 (1 mol%) is only present in the LUV. The lateral mobility of labeled DOPE obtained at both symmetric (open spheres) and asymmetric (closed spheres) lipid bilayers for different bilayer compositions are presented in Figure 2.

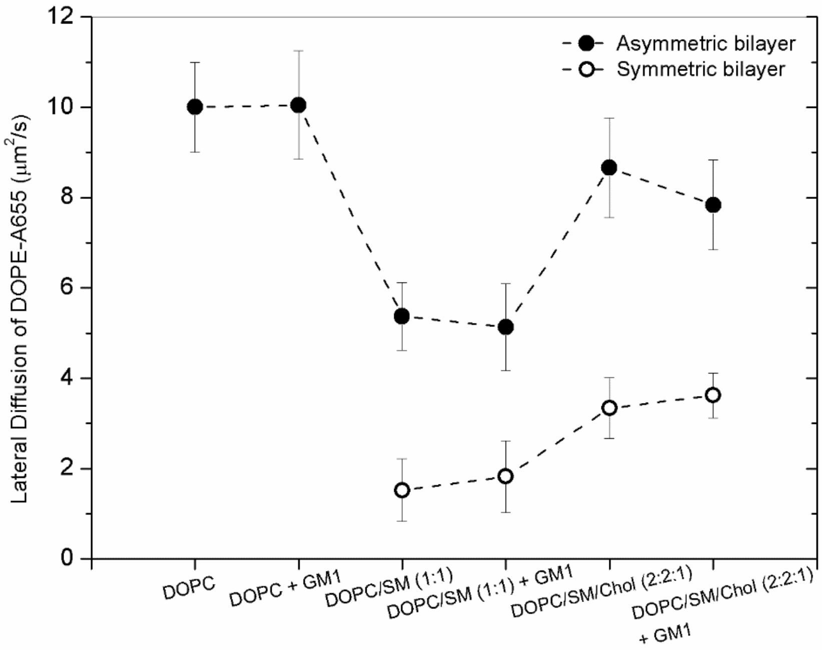

Figure 2. Lateral diffusion of labeled DOPE at asymmetric (closed spheres) and symmetric (open spheres) lipid bilayers. For the asymmetric bilayers, the proximal leaflet is comprised of DOPC. In each case, the mean diffusivity values presented herein are averages from 40 to 50 points (cavities) obtained across three independent bilayers. The experiments were performed at 20 ± 0.5 °C.

In all cases, it is the distal leaflet that is fluorescently labeled. The composition of the lower leaflet dramatically impacts diffusion of the upper leaflet. In symmetric lipid bilayers composed of DOPC/SM (1:1) the lateral diffusion coefficient of DOPE-A655 labeled at the distal leaflet is 1.52 ± 0.69 $\mu m^2 s^{-1}$, showing diffusion is significantly slowed compared with its asymmetric analogue (5.37 ± 0.75 $\mu m^2 s^{-1}$). This distinction indicates the integrity of the lipid distribution in the asymmetric bilayers and reflects the impact of inter-leaflet coupling in dictating membrane diffusion.

In the presence of cholesterol, i.e., in MSLBs with symmetric composition of DOPC/SM/Chol (2:2:1) in each leaflet, the lateral mobility of DOPE-A655 was measured as 3.34 ± 0.67 $\mu m^2 s^{-1}$ which is approximately 2.5 times slower than the asymmetric analogue (8.66 ± 2.53 $\mu m^2 s^{-1}$). Notably, inclusion of 1 mol% GM1 at the distal leaflet does not measurably alter DOPE-A655 diffusion coefficient irrespective of the membrane composition or symmetry.

Overall, our data indicate that it is possible to build stable asymmetric microcavity supported lipid bilayers and that the implicit fluidity of the MSLBs enables the facile study of diffusion as a function of different lipid composition. The data reflect the profound impact of leaflet asymmetry on membrane fluidity at both gel phase containing and in phase-separated lipid compositions. The magnitude of the change in fluidity between asymmetric and symmetric bilayers ($\Delta D = D_{asym}-D_{sym}$) is greater for binary fluid-gel phase membrane ΔD=3.6 $\mu m^2 s^{-1}$ than for fluid-fluid phase separated ternary membrane (ΔD = 2.6 $\mu m^2 s^{-1}$).

The decreased fluidity observed in symmetric bilayers is in agreement with computational predictions and with previous observations on liposomes where comparable differences in lipid lateral diffusion at symmetric and asymmetric were observed at similar temperatures.[37,8] For supported lipid bilayer systems based on solid substrate-supports, confounding surface-membrane frictional interactions complicate the interpretation of membrane viscosity as both inter-leaflet and substrate friction contribute to the measured viscosity.[38]

The viscosity values as estimated from the Saffman-Delbrück model (eq (5)) for the asymmetric and symmetric lipid bilayers are displayed in Table 1. We assume that the lipid bilayers spanned across the microcavity are planar. Although reported membrane viscosity values vary due to varying experimental conditions, such as lipid composition, temperature and bilayer model,[39] the viscosity values obtained herein lie within the range of previously literature reports, between 0.02 and 0.5 Pa.s.[40] The membrane viscosity calculated for DOPC with GM1 (1 mol%) present in the distal leaflet is comparable to previous data reported for DOPC lipid membranes.[41] The viscosity calculated for the asymmetric lipid bilayers comprised of DOPC//DOPC/SM (1:1) 0.1 Pa.s are decreased as expected but nonetheless lie within membrane viscosity ranges reported previously.[42] On the addition of cholesterol, the membrane viscosity decreases to 0.06 Pa.s which is anticipated since cholesterol increases membrane fluidity in lipid bilayers containing sphingomyelin. As expected from the FLCS data, lipid leaflet asymmetry exerts a profound influence on the membrane viscosity; the viscosity of the symmetric DOPC/SM(1:1) with 1 mol% GM1 is four times more viscous than that of its asymmetric counterparts.. The effect is less pronounced in the cholesterol-containing bilayer where the viscosity in the symmetric composition is 2.5 greater than the asymmetric layer. This indicates, again that there is significant frictional or inter-leaflet coupling transmitted through the membrane.

Protein assembly, detection and dynamics using highly versatile MSLBs

Next, we assessed the suitability of MSLBs as a platform to study GSL-protein interactions, by modeling the GM1-cholera toxin interaction. GSLs are important receptors for lectin-binding that reside in cells exclusively at exofacial leaflet of mammalian membranes where they can participate in remodeling and crosslinking of domains on receptor binding.[25] Fluidity is important in artificial platforms that model such behaviors as lateral diffusion of the participating players are required for remodeling. We examined here, the impact of GSL-toxin recognition on lipid membrane impedance and fluidity as a function of membrane trans-leaflet composition.

The impact of GSL-protein recognition on electrochemical properties of the MSLB:

The gold microcavity arrays (Figure 3a) that were selectively modified at the top surface with a 6-Mercapto-1-hexanol (MH) self-assembled monolayers using the PS sphere templates as a mask as described previously[43] and also presented in supplemental materials. A schematic representation of the MSLBs on gold substrate is shown in Figure 3b. The EIS data accrued from MSLB fitted to a heuristic model circuit (Figure 3c) as described previously for the MSLB.[20]. As shown in Figure 3d, before PS templating sphere removal, there is a finite resistance ($R_{\mathrm{SAM+PS}}$=1317Ω, data not shown) which decreases to 440Ω (R_{SAM}) upon PS removal (grey symbol) indicating increased access of redox probe to the cavity, but the resistance is considerably greater than the unmodified electrodes, confirming, consistent with previous measurements, that the gold of the cavities are exposed whilst the SAM remains intact at the top interface. The cavities are filled with PBS buffer and the substrate was always kept in contact with PBS buffer for further use in bilayer fabrication.

EIS provides complementary insights to the FLCS studies, by interrogating the electrical properties of the bilayer membranes in terms of capacitive and resistive changes. These parameters, in turn, reflect changes to aqueous/ionic permeability in response to CTb surface binding and aggregation to GM1. Figure 3c shows representative EIS plots before and after CTb exposure to the asymmetric MSLBs comprised of DOPC in the proximal and DOPC/SM/Chol (2:2:1) with additional 1 mol% GM1 in the distal leaflet of the bilayer. The complex impedance (Nyquist plot) is presented as the sum of the real, Z', and the imaginary, $-Z''$ components that originate mainly from the resistance and capacitance respectively of the measured electrochemical system.

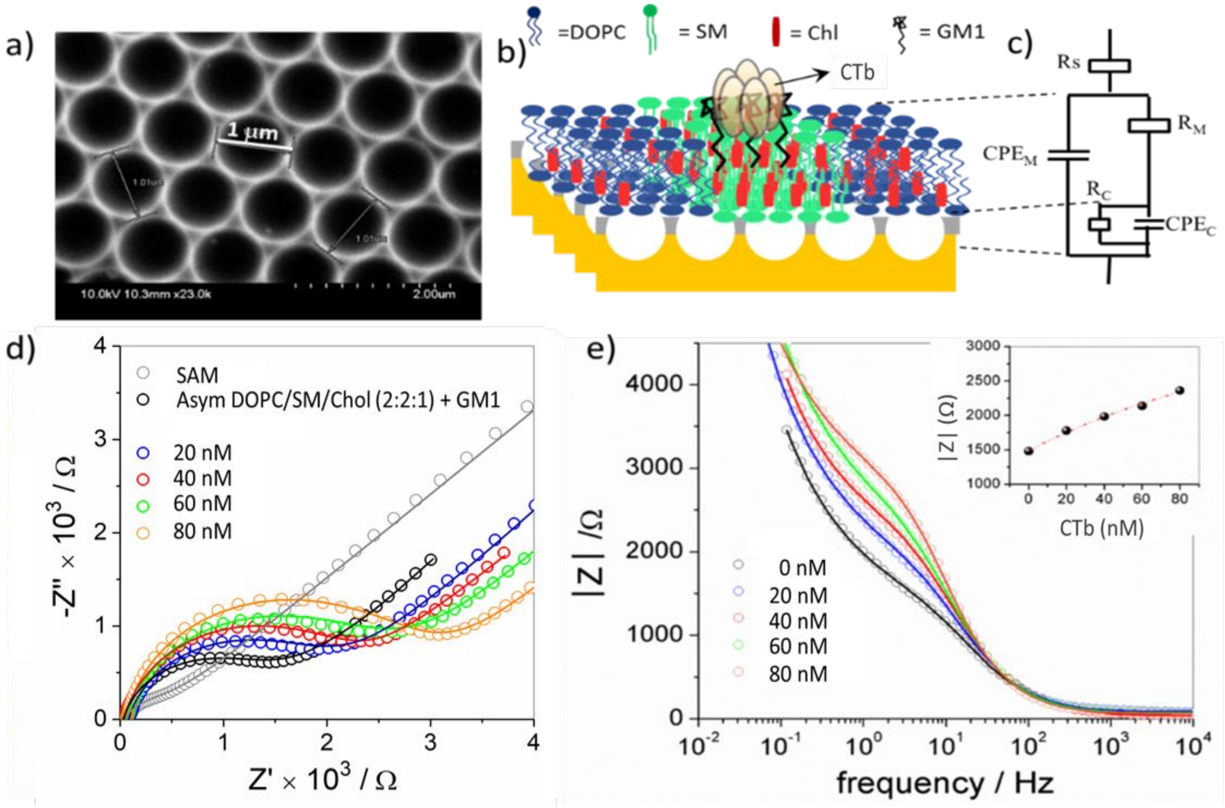

Figure 3. (a) SEM image of hemisphere micro cavity array obtained from electrochemical deposition through templates assembled from ~ 1μm diameter polystyrene spheres on gold substrates. (b) Schematic representation of MSLBs with CTb binding. (c) Represents the equivalent circuit model used to fit EIS data; where R_S: electrolyte solution resistane, R_M and CPE_M represent the membrane resistance and constant phase element, and R_C and CPE_C represent the resistance and constant phase element of cavity array. (d) Nyquist plot of microcavity gold electrode modified with MH SAM (light gray) prior to bilayer formation. Open black symbols show the EIS data of the cavity modified with asymmetric bilayers composed of proximal leaflet, DOPC and distal leaflet, DOPC/SM/Chol (2:2:1) with GM1 (1 mol%) and EIS spectra with different CTb concentration (blue: 20 nM, red: 40 nM, green, 60

nM, orange, 80 nM). (e) Magnitude of total impedance before and after CTb binding. Inset shows total impedance at a fixed frequency (4 Hz) as a function of the CTb concentration. All the EIS spectra recorded in the presence of 1 mM $Fe(CN)_6{}^{3-/4-}$ and 0.1 M KCl at the potential of +0.26 V vs. Ag/AgCl and frequency range of 10^4 to 0.01 Hz using a three-electrode setup consisting of a platinum counter, Ag/AgCl reference, and the microcavity array as working electrode.

The Nyquist plot for the gold microcavity electrode selectively modified with MH monolayer appears as a semicircle near the origin, at high frequencies, corresponding to heterogeneous electron transfer limited process, whereas the linear portion of the plot, at lower frequencies, represents the diffusion-controlled electron transfer process (Figure 3d, light grey). The assembly of the bilayer yields similar impedance curves but decreasing double layer capacitance due to retardation of the interfacial electron transfer rates compared to a bare or selectively modified metal electrode. This is reflected in the increase in semicircle diameter (black open symbol) in Figure 3d. Exposing the GM1 containing bilayer to increasing concentrations of CTb increases the semicircle diameter systematically and the data can be fit adequately by the Randles circuit as shown in Figure 3c. Since the membrane is a perfect resistance-capacitance element, the resistance is directly, and the capacitance inversely, proportional to the thickness of the dielectric layer. The parameter β of CPE_M in Eq. (1) is close to unity and hence a constant phase element, CPE_M could be used as a good representation of the electrode capacitance. From the fitting, the absolute resistance and capacitance of the asymmetric DOPC//DOPC/SM/Chol (2:2:1) with GM1 (1 mol%) at the outer leaflet, was found to be ~1.5 ± 0.06 kΩ.cm^2 and 1.4 ± 0.01 μF/cm^2 respectively which is in line with previous reports.[44,45] The relative change in resistance and capacitance values before and after toxin addition extracted from the fit are summarized in Table 2. We compare relative change rather than absolute C and R values as initial resistance values vary modestly from substrate to substrate for identical bilayer compositions due to small variations in the uniformity of cavity packing and electrode dimensions. We compared data across several replicate substrates and report the average relative changes in bilayer resistance and capacitance.

Table 2. Resistance and capacitance data for MSLBs at a fixed concentration (40 nM) of CTb. Results presented reflect the change (Δ) recorded following CTb addition, relative to bilayer prior to CTb addition. Asym indicates a bilayer that has a DOPC-only proximal leaflet, Sym indicates the bilayer is symmetric composition but for GM1 which in all compositions is only present at the outer leaflet.

Lipid composition	ΔR (kΩ.cm^2)	ΔC (μF/cm^2)
Sym DOPC + GM1 (1 mol%)	0.22 ± 0.01	-0.90 ± 0.15
Asym DOPC/SM/Chol (2:2:1) + GM1 (1 mol%)	0.87 ± 0.02	-0.80 ± 0.23
Sym DOPC/SM/Chol (2:2:1) + GM1 (1 mol%)	2.68 ± 0.13	-0.82 ± 0.24

As shown in Table 3, increasing CTb concentration in the solution in contact with the bilayer leads to a systematic increase in membrane resistance. The change in resistance is defined as $\Delta R = \Delta R_{CTb}-\Delta R_0$, where ΔR_{CTb} and ΔR_0 is the membrane resistance in the presence and in the absence of toxin respectively. Conversely, the capacitance ($\Delta C = \Delta C_{CTb}-\Delta C_0$) decreases systemically with increasing CTb concentration. Figure 3e represents the total impedance of the MSLBs as a function of increased concentration of CTb. At a fixed frequency of 4 Hz, the impedance rises with increasing CTb concentration (inset Figure 3e).

Table 3. Effect of CTb on the resistance and capacitance of asymmetric DOPC/SM/Chol (2:2:1) + GM1 (1 mol%) bilayer at increasing concentration. Results indicate change (Δ) recorded following CTb addition, relative to bilayer prior to CTb interaction.

[CTb] / nM	Asym DOPC/SM/Chol (2:2:1 mol/mol/mol) + GM1 (1 mol%)	
	ΔR (kΩcm^2)	ΔC (μF/cm^2)
0	0	0
20	0.42 ± 0.01	-0.4 ± 0.11
40	0.87 ± 0.02	-0.8 ± 0.23
60	0.96 ± 0.02	-1.7 ± 0.34
80	1.31 ± 0.015	-3.4 ± 0.42

In order to confirm CTb recognition by GM1 is specific, we carried out control experiments to evaluate impedance changes on exposure of CTb to DOPC and ternary DOPC/SM/Chol bilayer membranes in the absence of GM1. In contrast to the DOPC containing GM1 bilayers, no significant changes to film resistance or capacitance was observed on exposure to CTb across any of the toxin concentrations explored in the absence of GM1 in the distal leaflet (Table S1 and Figures S5a). These results confirm that the presence of GM1 in the distal leaflet is necessary for CTb binding. Conversely, for the symmetric ternary bilayer composed of DOPC/SM/Chol (2:2:1) with GM1 (1 mol%) at the distal leaflet, upon addition of 40 nM CTb, the relative change in resistance and capacitance was found to be 2.68±0.13 kΩcm^2 and -0.6±0.24 μFcm^{-2} respectively (Table 2). This reflects the large increases in bilayer resistance and decreases to the capacitance that accompanies exposure to CTb at both DOPC and ternary bilayer membranes in the presence of GM1. The magnitude of the changes is much greater for the SM containing bilayers and are consistent with the formation of a resistive layer of toxin at the membrane interface that leads to an increase in film thickness reflected in the capacitance decrease. Note that, the magnitude of change in absolute resistance for symmetric DOPC/SM/Chol (2:2:1) with GM1 (1 mol%) composition (~4.01 kΩcm^2) is higher than the asymmetric DOPC//DOPC/SM/Chol (2:2:1) with GM1 (1 mol%) composition (1.5 kΩcm^2). Resistance is notably greatest when both leaflets comprise domain forming lipids. That much lower resistance values are observed for the asymmetric systems again, confirms the asymmetry of the bilayers achieved at the MSLBs[46–49]. The greater resistance of domain forming bilayers is likey attributed to organization/tight packing of lipid bilayers propagated longitudinally along both leaflets. Interestingly, when there is no GM1 present for symmetric ternary bilayer (DOPC/SM/Chol), the resistance of the membrane was found to be 3.16±0.05 kΩcm^2 in the absence of toxin, increasing in the presence of CTb to 3.82 ±0.05 kΩcm^2 (Figure S5b). This contrasted with the DOPC-only bilayer where in the absence of GM1, CTb elicited no change to membrane impedance (Figure S5a). The change suggests that CTb is associating with the membrane when SM is present but GM1 is not. These results are further supported by FLCS studies, below, that show retardation of toxin diffusivity when exposed to SM containing bilayers in the absence of GM1 (Figure S5c, Table S1).

.

Lateral mobility of the CTb-GM1 complex is dependent on transmembrane composition:

Labeled CTb-A555 was used to directly monitor the protein diffusion by FLCS on exposure to GM1-containing membrane binding. The labeled toxin, dissolved in PBS buffer (pH 7.4) at 4 nM was injected into the MSLB contacting solution in the microfluidic device and incubated for 30 min to ensure equilibrium is reached.[50,51] Figure 4 a and b shows the reflectance and fluorescence images respectively obtained following CTb incubation at a DOPC MSLB containing 1mol% GM1 at the distal interface. The corresponding FLCS data shown in Table 4.

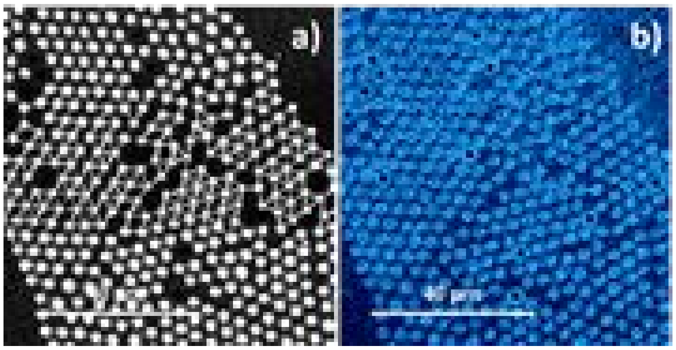

Figure 4. Representative confocal microscopy images obtained for labeled CTb-A555 of asymmetric DOPC + GM1 (1 mol%) lipid bilayer. (a) shows the reflectance image using OD3 filter before inserting labeled CTb. (b) shows the fluorescence lifetime image after incubating the lipid bilayer with 4 nm labeled CTb for 30min. The scale bar is 40 μm.

As the DOPC + GM1 (1 mol% at the outer leaflet) MSLB shown in Figure 4 is otherwise unlabeled we can conclude from imaging that the intense emission localized at the membrane following CTb incubation is due to toxin associating with the GM1-containing bilayer. The FLCS ACF (cf. Fig. 1e) accrued from the pore spanned membrane fit to a single component 2D diffusion model and the diffusion coefficient for the toxin is determined to be 5.65 ± 0.75 $\mu m^2 s^{-1}$. This value is approximately half that of the lipid marker which is consistent with the values reported for CTb assembly at GM1/DOPC giant unilamellar vesicles (GUVs).[52] As expected, the diffusion coefficient for MSLB membrane-bound CTb is significantly higher than values reported from SLBs with similar lipid bilayer composition. For instance, the lateral diffusion coefficient obtained for labeled CTb in supported lipid bilayers on silica substrate containing GM1 (0.1 mol%) was reported as 0.12 ± 0.03 $\mu m^2 s^{-1}$, measured by FRAP [53] and using STED/FCS, Honigmann *et al.* reported the lateral diffusion of CTb as 0.14 ± 0.01 $\mu m^2 s^{-1}$ for glass supported lipid bilayers.[54] The data reported here reflect the advantageous fluidity of the MSLBs compared to SLBs.

In asymmetric MSLBs comprised of DOPC/SM (1:1) with GM1 (1 mol%) at the distal leaflet and DOPC at the proximal, the ACF obtained for labeled CTb showed two diffusing populations. Fitting to a two-component model, equation 4, the populations contributed equally to the CTb fit with diffusion coefficients determined as 1.47 ± 0.40 $\mu m^2 s^{-1}$ and 0.03 ± 0.02 $\mu m^2 s^{-1}$. Recalling that lipid marker diffusion for the DOPC/SM (1:1 mol/mol) + GM1 (1 mol%) composition as 5.13 ± 0.96 $\mu m^2/s$, the diffusion coefficient of the fast component for CTb diffusion is five times slower than the lipid marker, rather than the half expected. The binary composition is expected to have co-existent liquid disordered and gel phases at 20±0.5 °C. The fast and slow diffusing components may be due to the toxin associated with GM1 localized in each phase.[55] However, given that the diffusion value is so much lower than the lipid marker for this composition and that the GM1 is expected to localize most strongly with the sphingomyelin (promoted through H-bonding) containing phase, it is more likely that the two populations reflect diffusion of CTb both at the gel phase but associated with different numbers of GM1. For the symmetric DOPC/SM bilayer (GM1 1 mol% in the distal leaflet) the lateral diffusion of CTb-GM1 complex is dramatically reduced and only a single diffusing population is evident. Indeed, diffusion is so slow that the intensity time trace shows strong photobleaching. This supports the argument that diffusion is due to two populations with different numbers of GM1 bound as only the gel phase would be expected to be so strongly affected by transverse lipid symmetry suggesting that the GM1-CTb complexes are confined to the sphingomyelin rich gel phase.

Next, we studied CTb binding at asymmetric phase-separated lipid bilayers where the distal lipid leaflet was composed of a DOPC/SM/Chol (2:2:1) + GM1 (1 mol%) and proximal DOPC only. The diffusivity of CTb fit well to a single component model and was determined as 3.26 ± 0.73 $\mu m^2\, s^{-1}$. Unlike DOPC bilayer, in the ternary bilayer the CTb diffusion coefficient was roughly half that of the diffusion coefficient of labeled lipid. Conversely, in the symmetric composition; both leaflets comprised of DOPC/SM/cholesterol (2:2:1) with GM1 (1 mol%) at the distal leaflet, the diffusivity of CTb (4nM) bound to GM1 is two orders of magnitude lower than the asymmetric lipid bilayer of the same composition. This dramatic impedance of diffusion suggests strongly that CTb-GM1 association occurs preferentially at the L_o phase, consistent with previous observations.[56,57] In addition the data may also suggest that both leaflets must have domain forming compositions for such phases to form, i.e. that domains are transmitted through both leaflets. Similar results of the influence of lipid composition on lateral CTb dynamics were noted by Burns *et al.* Using FCS, they showed that the lateral diffusion of labeled CTb-Alexa 488 was 0.040 $\mu m^2 s^{-1}$ after binding to GM1 in domain forming membranes in SLBs.[57]

Table 4. Effect of lipid composition on the lateral diffusion of CTb in symmetric and asymmetric MSLBs lipid compositions. GM1 at 1 mol% was present only in the distal lipid leaflet. The experiments were performed at 20 ± 0.5 °C.

Lipid composition	CTb lateral diffusion ($\mu m^2\ s^{-1}$)
Sym DOPC + GM1	5.6 ± 0.7
Asym DOPC/SM/Chol (2:2:1) + GM1	3.3 ± 0.7
Asym DOPC/SM (1:1) + GM1	1.47 ± 0.40; 0.03 ± 0.02
Sym DOPC/SM/Chol (2:2:1) + GM1	0.61 ± 0.12
Sym DOPC/SM (1:1) + GM1	0.05 ± 0.08

To determine if non-specific CTb adsorption at the membrane in the absence of GM1 occurs, control experiments were performed by FLCS and confocal fluorescence imaging. After extensive incubation of CTb at DOPC-only membranes, consistent with the EIS experiments, there was no evidence of CTb binding at the membrane. In contrast, however, CTb (4nM) was observed to adsorb at SM-containing bilayer in the absence of GM1. At DOPC/SM (1:1) binary membrane, we observe imaging emission from bound labeled CTb, and FLCS revealed a diffusion coefficient of 4.6 ± 1.8 $\mu m^2 s^{-1}$ and 3.1 ± 1.5 $\mu m^2 s^{-1}$ for CTb at the asymmetric and symmetric SM-containing bilayers respectively. Upon incubation at a ternary symmetric DOPC/SM/Chol (2:2:1) bilayer, CTb was also found to be associated and exhibited a diffusivity of 1.50 ± 0.20 $\mu m^2 s^{-1}$ (See Supplementary Information, Figure S5 and Table S1). Notably, the diffusion values are roughly half that observed for the toxin when GM1 is present, and correspond more closely with the diffusion values of the lipid label. Analogous behavior is evident at the ternary compositions in the absence of GM1, but our data that whereas SM must be present, cholesterol does not need to be present for CTb adsorption to occur The mechanism behind CTb interaction at SM containing bilayers is unknown but given the correlation between the diffusion rates of bound CTb and lipid, it is likely mediated by a direct single SM-CTb interaction. Given the propensity of SM to H-bond, perhaps this plays a role. To our knowledge, there are no previous reports of CTb association with sphingolipid although, SM interaction with other AB toxins has been proposed noted.[24,58]

From FLIM the average lifetime of the CTb-A555 on GM1 binding was also collected. The toxin bound A555 probe exhibits dual exponential fluorescence decay kinetics in all cases. In PBS (pH 7.4) buffer, away from membrane, τ1 was determined as 1.90 ns and τ2 as 0.54 ns (amplitude of 10% and 90% respectively), which is similar to previous data obtained for bioconjugated Alexa 555 dye.[59] On association with the GM1 at the lipid membrane the fluorescent lifetime, particularly of the longer lived, lower amplitude component was significantly extended as shown in Table S2. For example, in DOPC bilayers with 1% GM1 at the distal leaflet, τ1 was determined as 3.1 ns and τ2 as 0.6 ns (amplitude of 20% and 80% respectively, Figure S6 and Table S2). There was a modest dependence of the long component on the bilayer composition, (supplemental materials) wherein ternary composition τ1 it was slightly shorter but the substantial extension to fluorescent lifetime in all cases on GSL binding, is a useful marker for GM1 association.

CTb concentration affects its lateral diffusion on lipid bilayers due to toxin clustering

CTb/GM1 complexes have been demonstrated to diffuse very slowly within the plasma membrane of live cells compared to other protein-lipid complexes including the Shiga toxin complex.[52] The restricted lateral diffusion of CTb/GM1 complexes has been attributed to interaction with actin and also seems to be associated with ATP-dependent processes, that affects the cytoskeletal structure.[60] However, contributions from cross-linking of lipid domains due to multivalent binding of CTb, or due to aggregation of CTb after binding to GM1 may also contribute to the anomalously low mobility of CTb/GM1 complex. As, using atomic force microscopy (AFM), Wang et al. demonstrated the presence of CTb aggregates on POPC/GM1 bilayer. To date however, there have been no reports on the effect of cholera-cholera aggregation following GM1 association on the lateral diffusion of the resulting aggregates in membranes.[61,62]

To this end, we performed FLCS measurements to interrogate the diffusion of CTb/GM1 as a function of membrane composition. We first monitored the change in lateral mobility of CTb-A555 as a function of increasing concentration of unlabelled CTb at membranes containing static concentrations of GM1. Next, we addressed how membrane fluidity influences CTb binding. This is of interest because previous studies have shown that CTb intoxication occurs mostly at lipid raft or L_o domains whereas depletion of cholesterol has been shown to enhance CTb/GM1 binding.[60,63] For the mixed bilayers, we used the asymmetric MSLB's to enable these studies, because their enhanced fluidity, ensured diffusion of even aggregated CTb was fast enough to be measurable, and examined two lipid compositions, DOPC alone and DOPC/SM, both containing GM1 in the distal leaflet. To understand if the aggregation is driven by GM1 concentration, we also compared two receptor densities (1 and 5 mol% GM1) at both lipid compositions.

The diffusion coefficient of labeled CTb-A555 (4 nM) was first measured following its incubation for 30 min at 20±0.5 °C at the aforementioned lipid bilayers. Because of the need for low luminophore levels in FLCS unlabeled CTb concentration was then increased systematically whilst holding the concentration of labeled toxin CTb-A555 constant at 4nM. Following each addition of unlabeled CTb, a minimum of 30 min incubation was allowed. We confirmed separately that beyond 30 minutes no further change to CTb-A555 diffusivity occurred. Figure 5a and b show representative ACF curves for CTb-A555 as a function of CTb concentration at the DOPC MSLB containing GM1 1 mol% and 5 mol% respectively. The diffusivity of CTb-A555 at 4 nM fit to a single component model and exhibited Brownian diffusion with a diffusion coefficient of 5 $\mu m^2 s^{-1}$ at 1 mol% GM1. Above 4nM CTb, aggregation of the toxin was evident from the ACFs with concurrent fast and slow component to the fit caused by photobleach of labeled CTb (Figure 5c and 5d). The slow component, on time scale of our experiments were essentially immobile. The diffusivity of the mobile CTb component is plotted versus CTb concentration in Figure 6.

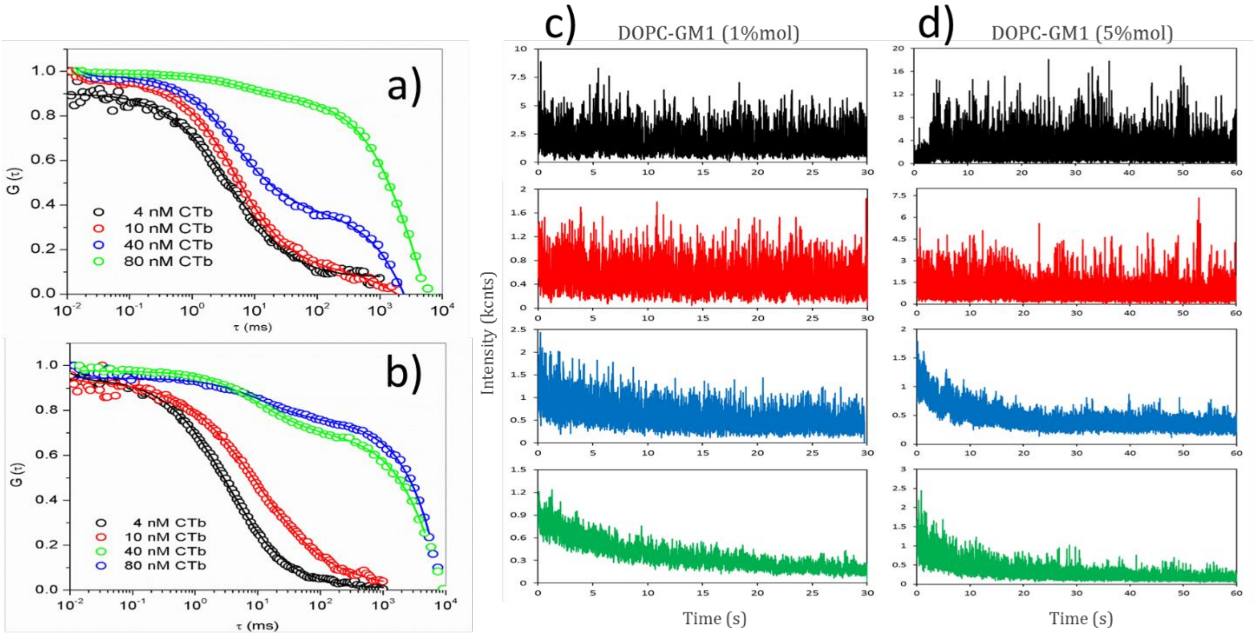

Figure 5. ACF and fluorescence intensity decay of CTb to an asymmetric DOPC lipid bilayer containing a) 1 and b) 5 mol% GM1 at distal leaflet at 20 °C. ACF curves in both panel at varied CTb concentrations are represented by 4 nM (black), 10 nM (red), 40 nM (blue) and 80 nM (green). Solid lines are the fitted data. CTb concentration of 10 nM, 40 nM and 80 nM were fitted with 2 diffusing components. The % contribution of the slow population (aggregates) to the ACF increases with GM1 concentration and CTb concentration. c) and d) represent the fluorescence intensity decay of labeled CTb-A555 at different unlabeled CTb concentration. Photobleaching induced by CTb aggregates can be observed at 40 nM (blue) and 80 nM (green) for both GM1 concentrations.

At DOPC MSLBs with 5 mol% GM1 at the distal leaflet, at 4 nM CTb, notably, D was considerably higher than for 1% GM1 at 8 $\mu m^2 s^{-1}$. Also, in contrast, at the 5 mol% GM1/DOPC membrane, the CTb diffusion remained single-component (Figure 6b) up to a CTb concentration of 10 nM indicating that the valency of GM1-CTb binding depends on GM1 concentration. At CTb concentrations greater than 10 nM, the ACF data again confirmed to a two-component fit and with decreasing diffusion coefficient in the fast component and increasing %P_{im} content. Although we were unable to estimate the diffusivity value for the immobile fraction because of photobleaching we were able to estimate its relative % contribution the signal and observed that it increased systematically from 0% at 4nM CTb to over 90% at 80 nM CTb for both GM1 concentrations. This very slow component is likely to be the crosslinked aggregates of CTb with multiple GM1 anchors. Estimation of diffusivity could be made for the fast diffusing fraction in the two-component fit (Figure 6) and this fraction is taken to be GM1 associated with varying number of GM1 anchors. The data shows that at simple DOPC bilayers the extent of CTb-GM1 aggregation depends directly on CTb concentration. And, that at lower concentrations of CTb the number of GM1 associating with the CTb appears to be greater at the1mol% GM1 compared with 5% mol. Our observations are consistent with previous reports, where increasing in GM1 content was observed to inhibit CTb binding.[64–66] However, at higher CTb concentrations, irrespective of GM1 concentration, the fast diffusing component is the same and extensive aggregation of the CTb has occurred.

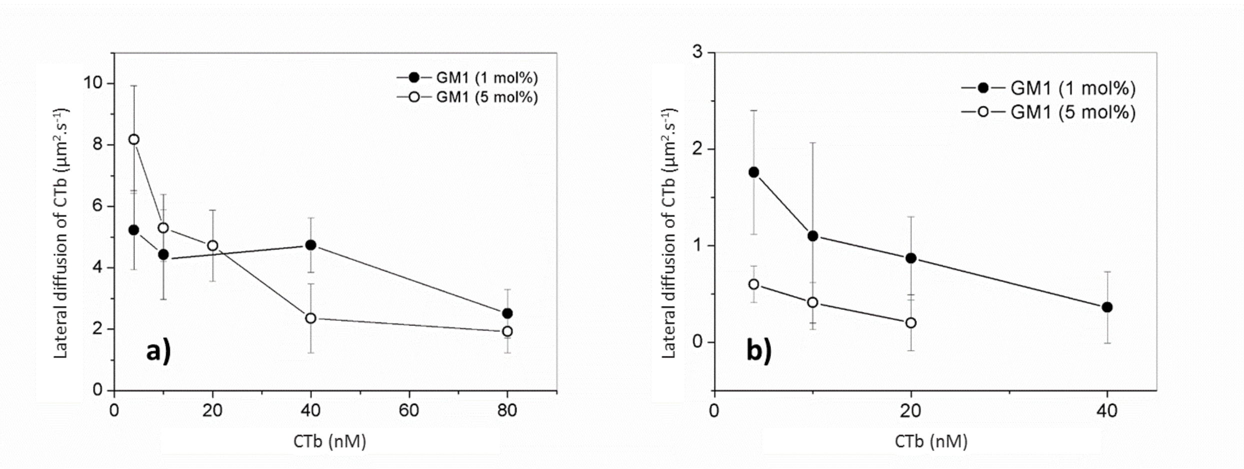

Figure 6. Diffusion of the fast component of CTb-A555 in presence of increasing concentrations of CTb for lipid bilayers containing 1 mol% (filled circles) and 5 mol% of GM1 (open circles) in the distal leaflet. (a) DOPC and (b) asymmetric DOPC/SM (1:1) mol/mol.

To further confirm that GM1-CTb clustering is occurring, GM1 diffusion was examined at a DOPC bilayer containing GM1 (1 mol %) at the distal leaflet containing 0.01 mol% GM1 alkyl tail labeled Bodipy-FL 488. Figure 7 shows the ACF of labeled GM1 before and after incubation with CTb (80 nM). The lateral diffusion of labeled GM1-488 in the distal leaflet in the absence of toxin was measured as 11.45 ± 3.55 $\mu m^2 s^{-1}$ (red symbols). Following incubation with unlabeled CTb (80 nM) the diffusion of GM1-488 became complex (green symbols) comprising a mobile and a slow-diffusing fraction. This behavior mirrors the diffusive behavior of the labeled CTb aggregation under the same conditions confirming the GM1 is participating in a GM1-CTb network.

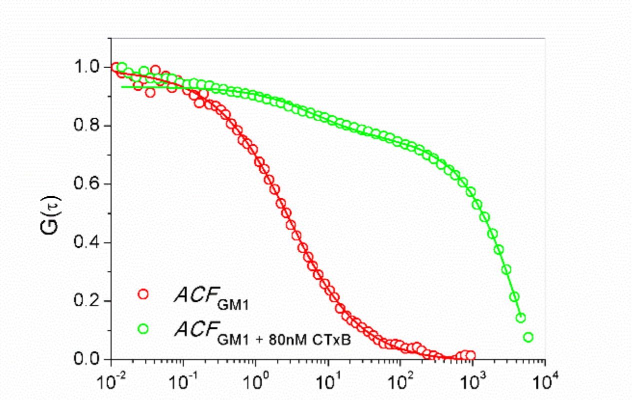

Figure 7. Autocorrelation functions (ACF) of labelled GM1-488 in asymmetric DOPC//DOPC+ GM1 (1 mol %) lipid membrane prior (red) and after incubation with 80 nM of unlabelled CTb (green). The shift to right represents the increasing of slow diffusing population, similarly to the labelled CTb scenario indicating that aggregation of CTb is dependent on protein concentration.

Effect of sphingomyelin on CTb binding within asymmetric lipid bilayers containing GM1

Concentration-dependent in-vitro studies of CTb binding due to GM1 clustering have focused on highly fluidic membranes comprised of DOPC and/or POPC.[61] To provide insight into the aggregation of CTb in SM containing membranes, we examined DOPC/SM (1:1) mixed lipid composition in the distal leaflet containing 1 mol% and 5 mol% of GM1 with DOPC in the proximal leaflet. The estimated diffusivity values for the toxin and the %P_{im} extracted from the fit to the ACF data are presented in Figure 8a and 8b and in Table S4. Initially, at 1 mol% GM1, the CTb response is strongly influenced by the presence of SM where even at 4 nm CTb concentration, a slow diffusing component and immobile/slow fraction constitute 50% of the population (Figure 8c), which is in agreement with previous studies reported by Schwille[52] and Kraut[67] showing that SM leads to immobilization of CTb. The CTb becomes completely immobile in the presence of 40 nM of unlabeled CTb, seen by the evolution of the ACF and fluorescence intensity of CTb-A555 (Figure 8 a and c). Similarly, for 5 mol % GM1, the fluorescence intensity fluctuations of CTb are affected by photobleaching (Figure 8b and Figure 8d). However, the % of immobile fraction increases with CTb concentration and is similarly evident even at 4 nM of CTb-A555, indicating that GM1 incorporates preferentially to SM to enriched gel domains and this can enhance CTb cross-linking of lipid domains. [68] Together with the non-selective adsorption of CTb at SM containing GM1-free bilayers this behavior may indicate that CTb clustering occurs in a cooperative manner with SM enriched domains and can be related to induced clustering of SM caused by CTb. Interestingly, unlike the DOPC-only bilayer higher GM1 concentration in the distal leaflet appear to enhance GM1 binding; the lateral diffusion of CTb-A555 (4 nM) was found to be $0.6 \pm 0.19\ \mu m^2 s^{-1}$ for 5 mol% GM1, which is approximately a 66% lower than diffusivity for the same bilayer at 1 mol% GM1 containing membrane (Figure 5b, Table S4).

Many authors report the bound CTb lateral diffusion as far slower than lipid markers in L_d or L_o regions in cells or GUVs.[52,69] Similarly our results obtained for symmetric lipid bilayers in particular, at MSLBs show immobility of CTb-GM1, suggesting extensive aggregation. Although asymmetric lipid bilayers also showed limited mobility which was rapidly diminished with increasing of CTb at the nanomolar range, we can propose that domain registry along with CTb and GM1 concentration contributes to the highly reduced CTb diffusion in cells and GUVs. Our data also indicate lipid diffusivity of DOPE-A655 was also altered by CTb binding but only for SM membranes (Table S4). This lateral mobility effect could be due to a lateral ordering of the lipid membrane dependently on CTb concentration as previously reported.[70] However, to the best of our knowledge, this is the first time that this effect is observed in an asymmetric lipid bilayer formed by a purely disordered DOPC lipid leaflet and a gel phase of DOPC containing SM lipid leaflet.

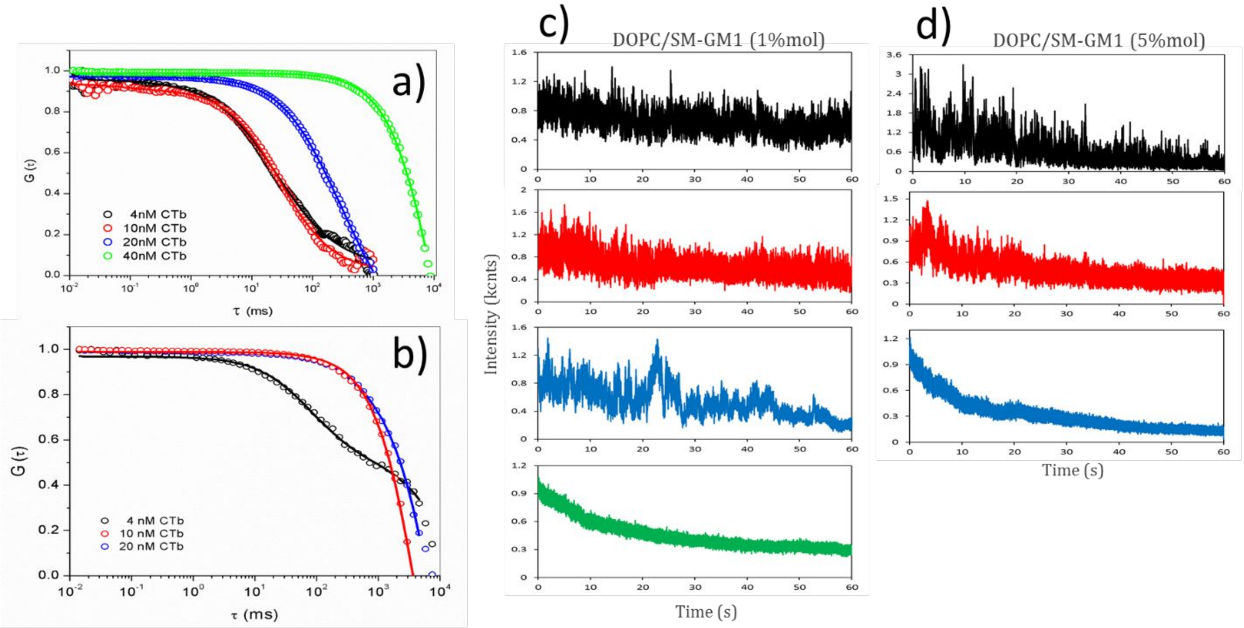

Figure 8. ACF and fluorescence intensity decay of CTb at an asymmetric lipid bilayer comprised of DOPC/SM (1:1 mol/mol) with GM1 (1 mol%), GM1 (5 mol%) studied by FLCS at 20 ±0.5 °C. a) and b) ACF curves obtained for 1 mol% and 5 mol% of GM1 respectively at 4 nM (black), 10 nM (red), 20 nM (blue) and 40 nM (green) of CTb with row data (dots) and fitting (solid line). CTb concentrations of 10 nM, 20 nM and 40 nM were fitted with 2 diffusing components. The % of slow diffusing population (aggregates) increases with GM1 concentration. c) and d) represent the fluorescence intensity decay of labeled CTb-A555 at

different wild type CTb concentration. Strong photobleaching induced by CTb aggregates is observed at 20nM (blue) and 40nM (green) for both GM1 concentrations.

CONCLUSIONS

The use of microcavity supported lipid bilayers as a platform to build transversally asymmetric lipid bilayer compositions and as a means to detect and study peripheral protein-membrane recognition at nanomolar range using EIS and FLCS at symmetric and asymmetric lipid bilayer compositions is reported.. Six membrane compositions were prepared using a combined Langmuir Blodgett - vesicle fusion method; Three symmetric bilayers: DOPC alone, a binary membrane contianing 1: 1 Sphingomyelin and DOPC as a model of mixed gel and L_d phase and a ternary phase separated DOPC:SM:Chol membrane containing fluid-fluid coexisting phases. Analogous asymmetric membranes in which the lower leaflet comprised DOPC were also prepared. . Fluorescence correlation spectroscopy demonstrated that transmembrane asymmetry has a profound influence on membrane fluidity. Where the gel phase and ternary compositions showed 2.5 to 3.5 times lower diffusion coefficient compared to their asymmetric analogues with a DOPC proximal leaflet.

The high fluidity of the asymmetric MSLBs enabled FLCS interogation into the effect of CTb binding on GM1-CTb aggregation, which was evaluated as a function of CTb concentration.. Following CTb administration two populations were found to contribute to the diffusion model.The % contribution of the slow diffusing fraction scaled with CTb concentration, suggesting it is CTb led -crosslinked aggregates, while the fast component % diminished and slowed with CTb concentration. This component was attributed to single CTb units anchored to 1, 2 or 3 GM1 units at the membrane, based on simple Saffman Delbrüch estimations of radii.

Notably, the data indicate that SM binds non-specifically to CTb perhaps contributing in a cooperative capacity to CTb GM1 binding at the membrane.

Gangliosides such as GM1 participate in a wide range of recognition and signalling processes at the cell membrane where signalling in many cases is driven by oligomerization or 2-dimensoinal network formation at the cell membrane. Modelling of such processes at artificial membrane requires capability to build transversally asymmetric bilayers but also fluidity is crucial to enable bilayer organisation. We demonstrate here that MSLBs are a versatile platform for evaluation of GSL-protein interactions at the lipid membrane that encompass these demands and permit multimodal detection methodologies in a single platform approach.

Notes

The authors declare no competing financial interest.

Supporting Information

Fabrication of gold and PDMS microcavity array substrates, Langmuir-Blodgetttransfer/vesicle disruptionmethod, FLCS calibration, additional FLCS and EIS data and analyses. This material is available free of charge via the Internet at http://pubs.acs.org.

Acknowledgment

This material is based upon work supported by Science Foundation Ireland under Grant No. [14/IA/2488] and the National Biophotonics and Imaging Platform, Ireland, funded by the Irish Government's Programme for Research in Third Level Institutions, Cycle 4 and 5, Ireland’s EU Structural Funds Programmes 2007-2013.

REFERENCES

(1) Schuster, B. S-Layer Protein-Based Biosensors. *Biosensors* **2018**, *8* (2). https://doi.org/10.3390/bios8020040.

(2) Siontorou, C. G.; Nikoleli, G.-P.; Nikolelis, D. P.; Karapetis, S. K. Artificial Lipid Membranes: Past, Present, and Future. *Membranes* **2017**, *7* (3), 38. https://doi.org/10.3390/membranes7030038.

(3) Espinosa, G.; López-Montero, I.; Monroy, F.; Langevin, D. Shear Rheology of Lipid Monolayers and Insights on Membrane Fluidity. *Proc. Natl. Acad. Sci.* **2011**, *108* (15), 6008–6013. https://doi.org/10.1073/pnas.1018572108.

(4) Engelman, D. M. Membranes Are More Mosaic than Fluid. *Nature* **2005**, *438*, 578–580. https://doi.org/10.1038/nature04394.

(5) Daleke, D. L. Regulation of Transbilayer Plasma Membrane Phospholipid Asymmetry. *J. Lipid Res.* **2003**, *44* (2), 233–242. https://doi.org/10.1194/jlr.R200019-JLR200.

(6) Marquardt, D.; Geier, B.; Pabst, G. Asymmetric Lipid Membranes: Towards More Realistic Model Systems. *Membranes* **2015**, *5* (2), 180–196. https://doi.org/10.3390/membranes5020180.

(7) Kiessling, V.; Wan, C.; Tamm, L. K. Domain Coupling in Asymmetric Lipid Bilayers. *Biochim. Biophys. Acta BBA - Biomembr.* **2009**, *1788* (1), 64–71. https://doi.org/10.1016/j.bbamem.2008.09.003.

(8) Perlmutter, J. D.; Sachs, J. N. Interleaflet Interaction and Asymmetry in Phase Separated Lipid Bilayers: Molecular Dynamics Simulations. *J. Am. Chem. Soc.* **2011**, *133* (17), 6563–6577. https://doi.org/10.1021/ja106626r.

(9) Crane, J. M.; Kiessling, V.; Tamm, L. K. Measuring Lipid Asymmetry in Planar Supported Bilayers by Fluorescence Interference Contrast Microscopy. *Langmuir* **2005**, *21* (4), 1377–1388. https://doi.org/10.1021/la047654w.

(10) Visco, I.; Chiantia, S.; Schwille, P. Asymmetric Supported Lipid Bilayer Formation via Methyl-β-Cyclodextrin Mediated Lipid Exchange: Influence of Asymmetry on Lipid Dynamics and Phase Behavior. *Langmuir* **2014**, *30* (25), 7475–7484. https://doi.org/10.1021/la500468r.

(11) Peyret, A.; Ibarboure, E.; Meins, J.-F. L.; Lecommandoux, S. Asymmetric Hybrid Polymer–Lipid Giant Vesicles as Cell Membrane Mimics. *Adv. Sci.* **2018**, *5* (1), 1700453. https://doi.org/10.1002/advs.201700453.

(12) Hwang, W. L.; Chen, M.; Cronin, B.; Holden, M. A.; Bayley, H. Asymmetric Droplet Interface Bilayers. *J. Am. Chem. Soc.* **2008**, *130* (18), 5878–5879. https://doi.org/10.1021/ja802089s.

(13) Raggers, R. J.; Pomorski, T.; Holthuis, J. C.; Kälin, N.; van Meer, G. Lipid Traffic: The ABC of Transbilayer Movement. *Traffic Cph. Den.* **2000**, *1* (3), 226–234.

(14) Chiantia, S.; London, E. Acyl Chain Length and Saturation Modulate Interleaflet Coupling in Asymmetric Bilayers: Effects on Dynamics and Structural Order. *Biophys. J.* **2012**, *103* (11), 2311–2319. https://doi.org/10.1016/j.bpj.2012.10.033.

(15) Przybylo, M.; Sýkora, J.; Humpolíčková, J.; Benda, A.; Zan, A.; Hof, M. Lipid Diffusion in Giant Unilamellar Vesicles Is More than 2 Times Faster than in Supported Phospholipid Bilayers under Identical Conditions. *Langmuir* **2006**, *22* (22), 9096–9099. https://doi.org/10.1021/la061934p.

(16) Schuster, B.; Weigert, S.; Pum, D.; Sára, M.; Sleytr, U. B. New Method for Generating Tetraether Lipid Membranes on Porous Supports. *Langmuir* **2003**, *19* (6), 2392–2397. https://doi.org/10.1021/la026691p.

(17) Schuster, B.; Sleytr, U. B. S-Layer-Supported Lipid Membranes. *Rev. Mol. Biotechnol.* **2000**, *74* (3), 233–254. https://doi.org/10.1016/S1389-0352(00)00014-3.

(18) Basit, H.; Gaul, V.; Maher, S.; Forster, R. J.; Keyes, T. E. Aqueous-Filled Polymer Microcavity Arrays: Versatile & Stable Lipid Bilayer Platforms Offering High Lateral Mobility to Incorporated Membrane Proteins. *The Analyst* **2015**, *140* (9), 3012–3018. https://doi.org/10.1039/C4AN02317J.

(19) Ogier, S. D.; Bushby, R. J.; Cheng, Y.; Evans, S. D.; Evans, S. W.; Jenkins, A. T. A.; Knowles, P. F.; Miles, R. E. Suspended Planar Phospholipid Bilayers on Micromachined Supports. *Langmuir* **2000**, *16* (13), 5696–5701. https://doi.org/10.1021/la991367o.

(20) Maher, S.; Basit, H.; Forster, R. J.; Keyes, T. E. Micron Dimensioned Cavity Array Supported Lipid Bilayers for the Electrochemical Investigation of Ionophore Activity. *Bioelectrochemistry* **2016**, *112*, 16–23. https://doi.org/10.1016/j.bioelechem.2016.07.002.

(21) Joubert, J. R.; Smith, K. A.; Johnson, E.; Keogh, J. P.; Wysocki, V. H.; Gale, B. K.; Conboy, J. C.; Saavedra, S. S. Stable, Ligand-Doped, Poly(Bis-SorbPC) Lipid Bilayer Arrays for Protein Binding and Detection. *ACS Appl. Mater. Interfaces* **2009**, *1* (6), 1310–1315. https://doi.org/10.1021/am900177p.

(22) Jobling, M. G.; Yang, Z.; Kam, W. R.; Lencer, W. I.; Holmes, R. K. A Single Native Ganglioside GM1-Binding Site Is Sufficient for Cholera Toxin To Bind to Cells and Complete the Intoxication Pathway. *mBio* **2012**, *3* (6). https://doi.org/10.1128/mBio.00401-12.

(23) Sezgin, E.; Schwille, P. Fluorescence Techniques to Study Lipid Dynamics. *Cold Spring Harb. Perspect. Biol.* **2011**, *3* (11). https://doi.org/10.1101/cshperspect.a009803.

(24) Reig, N.; van der Goot, F. G. About Lipids and Toxins. *FEBS Lett.* **2006**, *580* (23), 5572–5579.

(25) Raghunathan, K.; Wong, T. H.; Chinnapen, D. J.; Lencer, W. I.; Jobling, M. G.; Kenworthy, A. K. Glycolipid Crosslinking Is Required for Cholera Toxin to Partition Into and Stabilize Ordered Domains. *Biophys. J.* **2016**, *111* (12), 2547–2550. https://doi.org/10.1016/j.bpj.2016.11.008.

(26) Johnson, S. A.; Stinson, B. M.; Go, M. S.; Carmona, L. M.; Reminick, J. I.; Fang, X.; Baumgart, T. Temperature-Dependent Phase Behavior and Protein Partitioning in Giant Plasma Membrane Vesicles. *Biochim. Biophys. Acta BBA - Biomembr.* **2010**, *1798* (7), 1427–1435. https://doi.org/10.1016/j.bbamem.2010.03.009.

(27) Basit, H.; Maher, S.; Forster, R. J.; Keyes, T. E. Electrochemically Triggered Release of Reagent to the Proximal Leaflet of a Microcavity Supported Lipid Bilayer. *Langmuir ACS J. Surf. Colloids* **2017**, *33* (27), 6691–6700. https://doi.org/10.1021/acs.langmuir.7b01069.

(28) Tabarin, T.; Martin, A.; Forster, R. J.; Keyes, T. E. Poly-Ethylene Glycol Induced Super-Diffusivity in Lipid Bilayer Membranes. *Soft Matter* **2012**, *8* (33), 8743–8751. https://doi.org/10.1039/C2SM25742D.

(29) Bennett, W. F. D.; MacCallum, J. L.; Hinner, M. J.; Marrink, S. J.; Tieleman, D. P. Molecular View of Cholesterol Flip-Flop and Chemical Potential in Different Membrane Environments. *J. Am. Chem. Soc.* **2009**, *131* (35), 12714–12720. https://doi.org/10.1021/ja903529f.

(30) van Meer, G. Dynamic Transbilayer Lipid Asymmetry. *Cold Spring Harb. Perspect. Biol.* **2011**, *3* (5), a004671–a004671. https://doi.org/10.1101/cshperspect.a004671.

(31) Heinemann, F.; Schwille, P. Preparation of Micrometer-Sized Free-Standing Membranes. *ChemPhysChem* **2011**, *12* (14), 2568–2571. https://doi.org/10.1002/cphc.201100438.

(32) Yokota, K.; Ogino, T. Phase Separation in Lipid Bilayer Membranes Induced by Intermixing at a Boundary of Two Phases with Different Components. *Chem. Phys. Lipids* **2015**, *191*, 147–152. https://doi.org/10.1016/j.chemphyslip.2015.09.001.

(33) Becucci, L.; Martinuzzi, S.; Monetti, E.; Mercatelli, R.; Quercioli, F.; Battistel, D.; Guidelli, R. Electrochemical Impedance Spectroscopy and Fluorescence Lifetime Imaging of Lipid Mixtures Self-Assembled on Mercury. *Soft Matter* **2010**, *6* (12), 2733–2741. https://doi.org/10.1039/B923895F.

(34) Baumgart, T.; Hunt, G.; Farkas, E. R.; Webb, W. W.; Feigenson, G. W. Fluorescence Probe Partitioning between Lo/Ld Phases in Lipid Membranes. *Biochim. Biophys. Acta* **2007**, *1768* (9), 2182–2194. https://doi.org/10.1016/j.bbamem.2007.05.012.

(35) Kahya, N.; Schwille, P. How Phospholipid-Cholesterol Interactions Modulate Lipid Lateral Diffusion, as Revealed by Fluorescence Correlation Spectroscopy. *J. Fluoresc.* **2006**, *16* (5), 671–678. https://doi.org/10.1007/s10895-006-0108-6.

(36) McMullen, T. P. W.; McElhaney, R. N. New Aspects of the Interaction of Cholesterol with Dipalmitoylphosphatidylcholine Bilayers as Revealed by High-Sensitivity Differential Scanning Calorimetry. *Biochim. Biophys. Acta BBA - Biomembr.* **1995**, *1234* (1), 90–98. https://doi.org/10.1016/0005-2736(94)00266-R.

(37) Lin, Q.; London, E. Ordered Raft Domains Induced by Outer Leaflet Sphingomyelin in Cholesterol-Rich Asymmetric Vesicles. *Biophys. J.* **2015**, *108* (9), 2212–2222. https://doi.org/10.1016/j.bpj.2015.03.056.

(38) Hill Reghan J.; Wang Chih-Ying. Diffusion in Phospholipid Bilayer Membranes: Dual-Leaflet Dynamics and the Roles of Tracer–Leaflet and Inter-Leaflet Coupling. *Proc. R. Soc. Math. Phys. Eng. Sci.* **2014**, *470* (2167), 20130843. https://doi.org/10.1098/rspa.2013.0843.

(39) Block, S. Brownian Motion at Lipid Membranes: A Comparison of Hydrodynamic Models Describing and Experiments Quantifying Diffusion within Lipid Bilayers. *Biomolecules* **2018**, *8* (2). https://doi.org/10.3390/biom8020030.

(40) Kuimova, M. K.; Yahioglu, G.; Levitt, J. A.; Suhling, K. Molecular Rotor Measures Viscosity of Live Cells via Fluorescence Lifetime Imaging. *J. Am. Chem. Soc.* **2008**, *130* (21), 6672–6673. https://doi.org/10.1021/ja800570d.

(41) Nojima, Y.; Iwata, K. Viscosity Heterogeneity inside Lipid Bilayers of Single-Component Phosphatidylcholine Liposomes Observed with Picosecond Time-Resolved Fluorescence Spectroscopy. *J. Phys. Chem. B* **2014**, *118* (29), 8631–8641. https://doi.org/10.1021/jp503921e.

(42) Ramadurai, S.; Holt, A.; Krasnikov, V.; van den Bogaart, G.; Killian, J. A.; Poolman, B. Lateral Diffusion of Membrane Proteins. *J. Am. Chem. Soc.* **2009**, *131* (35), 12650–12656.

(43) Adamson, K.; Spain, E.; Prendergast, U.; Moran, N.; Forster, R. J.; Keyes, T. E. Fibrinogen Motif Discriminates Platelet and Cell Capture in Peptide-Modified Gold Micropore Arrays. *Langmuir* **2018**, *34* (2), 715–725. https://doi.org/10.1021/acs.langmuir.7b03279.

(44) Nascimento, J. M.; Franco, O. L.; Oliveira, M. D. L.; Andrade, C. A. S. Evaluation of Magainin I Interactions with Lipid Membranes: An Optical and Electrochemical Study. *Chem. Phys. Lipids* **2012**, *165* (5), 537–544. https://doi.org/10.1016/j.chemphyslip.2012.05.002.

(45) Juhaniewicz, J.; Sek, S. Interaction of Melittin with Negatively Charged Lipid Bilayers Supported on Gold Electrodes. *Electrochimica Acta* **2016**, *197*, 336–343. https://doi.org/10.1016/j.electacta.2015.11.134.

(46) Collins, M. D. Interleaflet Coupling Mechanisms in Bilayers of Lipids and Cholesterol. *Biophys. J.* **2008**, *94* (5), L32–L34. https://doi.org/10.1529/biophysj.107.124362.

(47) Garg, S.; Rühe, J.; Lüdtke, K.; Jordan, R.; Naumann, C. A. Domain Registration in Raft-Mimicking Lipid Mixtures Studied Using Polymer-Tethered Lipid Bilayers. *Biophys. J.* **2007**, *92* (4), 1263–1270. https://doi.org/10.1529/biophysj.106.091082.

(48) Kiessling, V.; Crane, J. M.; Tamm, L. K. Transbilayer Effects of Raft-like Lipid Domains in Asymmetric Planar Bilayers Measured by Single Molecule Tracking. *Biophys. J.* **2006**, *91* (9), 3313–3326. https://doi.org/10.1529/biophysj.106.091421.

(49) Putzel, G. G.; Uline, M. J.; Szleifer, I.; Schick, M. Interleaflet Coupling and Domain Registry in Phase-Separated Lipid Bilayers. *Biophys. J.* **2011**, *100* (4), 996–1004. https://doi.org/10.1016/j.bpj.2011.01.021.

(50) Heinemann, F.; Vogel, S. K.; Schwille, P. Lateral Membrane Diffusion Modulated by a Minimal Actin Cortex. *Biophys. J.* **2013**, *104* (7), 1465–1475. https://doi.org/10.1016/j.bpj.2013.02.042.

(51) Lauer, S.; Goldstein, B.; Nolan, R. L.; Nolan, J. P. Analysis of Cholera Toxin-Ganglioside Interactions by Flow Cytometry. *Biochemistry* **2002**, *41* (6), 1742–1751.

(52) Bacia, K.; Scherfeld, D.; Kahya, N.; Schwille, P. Fluorescence Correlation Spectroscopy Relates Rafts in Model and Native Membranes. *Biophys. J.* **2004**, *87* (2), 1034–1043. https://doi.org/10.1529/biophysj.104.040519.

(53) Kelly, C. V.; Wakefield, D. L.; Holowka, D. A.; Craighead, H. G.; Baird, B. A. Near-Field Fluorescence Cross-Correlation Spectroscopy on Planar Membranes. *ACS Nano* **2014**, *8* (7), 7392–7404. https://doi.org/10.1021/nn502593k.

(54) Honigmann, A.; Mueller, V.; Ta, H.; Schoenle, A.; Sezgin, E.; Hell, S. W.; Eggeling, C. Scanning STED-FCS Reveals Spatiotemporal Heterogeneity of Lipid Interaction in the Plasma Membrane of Living Cells. *Nat. Commun.* **2014**, *5*, 5412. https://doi.org/10.1038/ncomms6412.

(55) Bezlyepkina, N.; Gracià, R. S.; Shchelokovskyy, P.; Lipowsky, R.; Dimova, R. Phase Diagram and Tie-Line Determination for the Ternary Mixture DOPC/ESM/Cholesterol. *Biophys. J.* **2013**, *104* (7), 1456–1464. https://doi.org/10.1016/j.bpj.2013.02.024.

(56) Levental, I.; Byfield, F. J.; Chowdhury, P.; Gai, F.; Baumgart, T.; Janmey, P. A. Cholesterol-Dependent Phase Separation in Cell-Derived Giant Plasma-Membrane Vesicles. *Biochem. J.* **2009**, *424* (2), 163–167. https://doi.org/10.1042/BJ20091283.

(57) Burns, A. R.; Frankel, D. J.; Buranda, T. Local Mobility in Lipid Domains of Supported Bilayers Characterized by Atomic Force Microscopy and Fluorescence Correlation Spectroscopy. *Biophys. J.* **2005**, *89* (2), 1081–1093. https://doi.org/10.1529/biophysj.105.060327.

(58) Brothers, M. C.; Ho, M.; Maharjan, R.; Clemons, N. C.; Bannai, Y.; Waites, M. A.; Faulkner, M. J.; Kuhlenschmidt, T. B.; Kuhlenschmidt, M. S.; Blanke, S. R.; Rienstra, C. M., Wilson, B. A. Membrane Interaction of Pasteurella Multocida Toxin Involves Sphingomyelin. *FEBS J.* **2011**, *278* (23), 4633–4648. https://doi.org/10.1111/j.1742-4658.2011.08365.x.

(59) Bumb, A.; Sarkar, S. K.; Wu, X. S.; Brechbiel, M. W.; Neuman, K. C. Quantitative Characterization of Fluorophores in Multi-Component Nanoprobes by Single-Molecule Fluorescence. *Biomed. Opt. Express* **2011**, *2* (10), 2761–2769. https://doi.org/10.1364/BOE.2.002761.

(60) Day, C. A.; Kenworthy, A. K. Mechanisms Underlying the Confined Diffusion of Cholera Toxin B-Subunit in Intact Cell Membranes. *PLoS ONE* **2012**, *7* (4). https://doi.org/10.1371/journal.pone.0034923.

(61) Wang, R.; Shi, J.; Parikh, A. N.; Shreve, A. P.; Chen, L.; Swanson, B. I. Evidence for Cholera Aggregation on GM1-Decorated Lipid Bilayers. *Colloids Surf. B Biointerfaces* **2004**, *33* (1), 45–51. https://doi.org/10.1016/j.colsurfb.2003.09.001.

(62) Mou, J.; Yang, J.; Shao, Z. Atomic Force Microscopy of Cholera Toxin B-Oligomers Bound to Bilayers of Biologically Relevant Lipids. *J. Mol. Biol.* **1995**, *248* (3), 507–512. https://doi.org/10.1006/jmbi.1995.0238.

(63) Terrell, J.; Yadava, P.; Castro, C.; Hughes, J. Liposome Fluidity Alters Interactions Between the Ganglioside GM1 and Cholera Toxin B Subunit. *J. Liposome Res.* **2008**, *18* (1), 21–29. https://doi.org/10.1080/08982100801893929.

(64) Shi, J.; Yang, T.; Kataoka, S.; Zhang, Y.; Diaz, A. J.; Cremer, P. S. GM $_1$ Clustering Inhibits Cholera Toxin Binding in Supported Phospholipid Membranes. *J. Am. Chem. Soc.* **2007**, *129* (18), 5954–5961. https://doi.org/10.1021/ja069375w.

(65) Šachl, R.; Amaro, M.; Aydogan, G.; Koukalová, A.; Mikhalyov, I. I.; Boldyrev, I. A.; Humpolíčková, J.; Hof, M. On Multivalent Receptor Activity of GM1 in Cholesterol Containing Membranes. *Biochim. Biophys. Acta BBA - Mol. Cell Res.* **2015**, *1853* (4), 850–857. https://doi.org/10.1016/j.bbamcr.2014.07.016.

(66) Sagle, L. B.; Ruvuna, L. K.; Bingham, J. M.; Liu, C.; Cremer, P. S.; Van Duyne, R. P. Single Plasmonic Nanoparticle Tracking Studies of Solid Supported Bilayers with Ganglioside Lipids. *J. Am. Chem. Soc.* **2012**, *134* (38), 15832–15839. https://doi.org/10.1021/ja3054095.

(67) Hebbar, S.; Lee, E.; Manna, M.; Steinert, S.; Kumar, G. S.; Wenk, M.; Wohland, T.; Kraut, R. A Fluorescent Sphingolipid Binding Domain Peptide Probe Interacts with Sphingolipids and Cholesterol-Dependent Raft Domains. *J. Lipid Res.* **2008**, *49* (5), 1077–1089. https://doi.org/10.1194/jlr.M700543-JLR200.

(68) Day, C. A.; Kenworthy, A. K. Functions of Cholera Toxin B-Subunit as a Raft Cross-Linker. *Essays Biochem.* **2015**, *57*, 135–145. https://doi.org/10.1042/bse0570135.

(69) Moens, P. D. J.; Digman, M. A.; Gratton, E. Modes of Diffusion of Cholera Toxin Bound to GM1 on Live Cell Membrane by Image Mean Square Displacement Analysis. *Biophys. J.* **2015**, *108* (6), 1448–1458. https://doi.org/10.1016/j.bpj.2015.02.003.

(70) Forstner, M. B.; Yee, C. K.; Parikh, A. N.; Groves, J. T. Lipid Lateral Mobility and Membrane Phase Structure Modulation by Protein Binding. *J. Am. Chem. Soc.* **2006**, *128* (47), 15221–15227. https://doi.org/10.1021/ja064093h.

Table of Contents Graphic